

EFFECT OF NANOSTRUCTURED SURFACES ON THE WATER NUCLEATE BOILING

L. V. HEITICH, J. C. PASSOS*, E. M. CARDOSO, A. N. KLEIN, A. RAINHO NETO

* Author for correspondence

Department of Mechanical Engineering, LEPTEN / Boiling, Laboratory of Process Engineering and Energy Technology, Federal University of Santa Catarina, Florianópolis, SC, Brazil,
e-mail: jpassos@emc.ufsc.br

ABSTRACT

The study of the effect of nanostructures on the nucleate boiling is motivated by previous research using nanofluids, which the results indicated surface modifications that can enhance or not the heat transfer coefficient and cause the augmentation of the critical heat flux and the consequent enhancement of the process.

The present work aims to analyze the effect of nanostructure surfaces on the nucleate boiling of distilled water, at saturation temperature and atmospheric pressure. The studied nanostructures consist of nanoparticles of molybdenum (obtained by the Sputtering method) and maghemite, deposited on the very thin tapes of Constantan substrate.

The results obtained with the nanostructures were compared with experimental results of the smooth and the rough tapes (substrate). The visualization of boiling phenomena was carried out by a high speed camera.

The nanostructures increased the surface wettability, especially for maghemite deposition, and consequently increased the values of critical heat flux. The increase in heat transfer coefficient was observed only for high heat fluxes. The measurement of the apparent contact angle showed that the rough substrates have high hydrophobic characteristics and an enhancement in the heat transfer coefficient.

Keywords: Nucleate boiling. Nano-structures. Nanofluids. Maghemite. Sputtering. Contact angle.

1. INTRODUCTION

The use of nanoparticles dispersed in a base fluid has attracted attention of researchers. The term nanofluid, described by Choi (1995), has based on the increase of the thermal properties compared to commonly used refrigerants. There seems to be a consensus among researchers, such as Golubovic et al. (2009), Kim et al. (2007) and Wen and Ding (2005), that the increase in wettability as a result of deposition of nanoparticles on the heated surface is responsible for increasing the critical heat flux (CHF). However, there are many controversies about the heat transfer coefficient. Wen and Ding (2005) observed in their studies an increase in the heat transfer as the contact angle decreased, but Bang and Chang (2005) showed degradation in the heat transfer with increasing wettability. These recent studies highlight the importance of nanoparticles deposition and the changes it causes on the wettability of the heated surface, suggesting that such depositions are responsible for the changes in the boiling process (Kim et al., 2009).

Properties achieved by nanomaterials make them of great interest in technology and subject of study in several research areas. The use of nanostructures in thermal processes, such as boiling, is motivated by the fact that nanoparticles deposited modify the characteristics of the heated surface and thus influence the process of heat transfer. The main change observed is in the contact angle, leaving the surface more hydrophilic or hydrophobic. Some authors attribute this effect to higher values in CHF using nanofluids.

Forrest et al. (2010) investigate pool boiling characteristics of polymer/SiO₂ nanoparticle multilayers applied to nickel wire in pure de-ionized water. The nanoparticle thin-film coatings exhibited hydrophilic or hydrophobic properties depending on the final treatment. The authors found that the CHF increased for all thin-film coatings tested. According to their experiments, the results support the importance of the receding contact angle on CHF, and that a low receding contact angle yields a higher CHF. The authors observed that, for the same heat flux value, the hydrophobic surface had the greatest enhancement in the nucleate boiling heat transfer coefficient, whereas the hydrophilic and superhydrophilic surfaces had a slight degradation.

Hendricks et al. (2010) studied a novel approach to fabricate unique nanostructured surfaces using ZnO and they observed an improvement in the heat transfer coefficient for the ZnO nanostructured surfaces when compared to plain surface. The authors attributed this improvement to a high nucleation site densities and bubble frequency at the surface. This work also demonstrated the dependence between the critical heat flux and the contact angle.

Ahn et al. (2010) studied the CHF increase in pool boiling on an anodizing surface of zircaloy-4. The results showed an increase in the CHF with a decrease in the contact angle and the authors suggested that this is not explained only by the wettability effect. Stutz et al. (2011) studied the effects of nanostructured surface of wire coatings on boiling heat transfer and CHF. The authors reported a significant increase in CHF, also attributed to the wettability. In addition, there was a reduction in the heat transfer coefficient, which was explained by the coating which causes a decrease in the heat transfer coefficient due to a thermal resistance that becomes more remarkable as layer thickness increasing.

The present work aims to analyze the effect of nanostructured surfaces on the water nucleate boiling process, at saturation temperature and at atmospheric pressure.

2. EXPERIMENTAL PROCEDURES

2.1. Experimental apparatus

The boiling chamber, Figure 1, consists of a boiling chamber installed in the center of an external chamber, both assembled between two horizontal stainless steel AISI 316 plates of 200 x 200 x 17mm. The boiling chamber is a vertical glass tube with an 83mm inner diameter and 150mm height, which contains the test section and the working fluid being inside. The tightness is

obtained with rubber insulating and vacuum grease. The test condition temperature of the working fluid is imposed by a forced flow of water in the space existing between the glass tube of the boiling chamber and the plexy-glass wall of the external chamber. Inside the boiling chamber, in the upper part, there is a serpentine heat exchanger cooled by water whose temperature is controlled by a second cryostat. A pressure transducer measures the pressure inside the boiling chamber and a valve is used for charging the test fluid to ensure the atmospheric pressure during the tests.

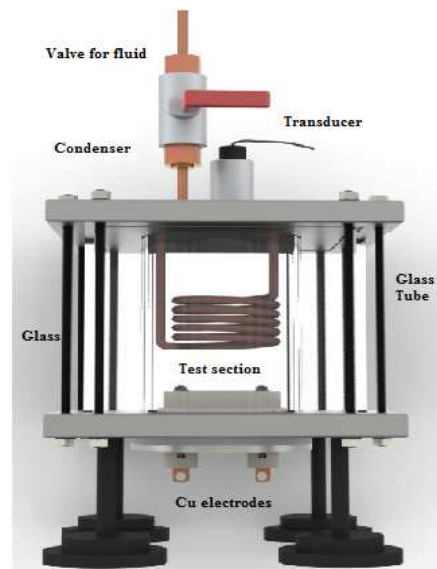


Figure 1. Boiling Chamber.

The test section, Figure 2a, consists of a Teflon base, with two copper electrodes connected to the power source, which allows the surface heating. The heated surface, Figure 2b, consists of a Constantan tape with 38mm length and 0.01 mm thickness, mounted on the PVC support and this, in turn, is fitted to the test section. The heating is done by Joule effect.

The tape is made of Constantan (55% Ni and 45% Cu) that has a high electrical resistivity ($51 \cdot 10^{-8} \Omega m$), compared to other metals such as copper. The Constantan tape is used as a substrate for all nanostructures used in the present work. Two E-type thermocouples, fixed in the Constantan tape, are used to determine the wall temperatures and the heat flux.

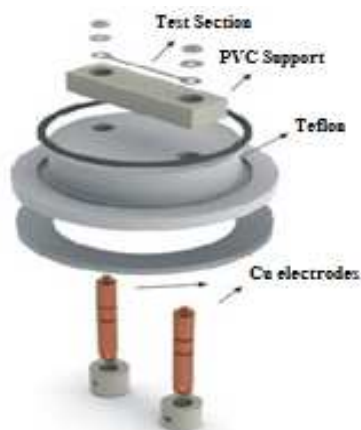


Figure 2a. View of test section assembly.

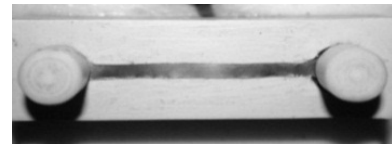


Figure 2b. Constantan tape on the PVC support.

2.2. Test Section Preparation

In this study were analyzed seven types of heated surface where four of them were nanostructured: smooth surface, rough surface, two heated surfaces with molybdenum deposition and the two other with maghemite deposition. Another type of heated surface tested was resultant from the boiling process of maghemite – water nanofluid.

The nanostructures are produced by the molybdenum nanoparticles deposition via Sputtering process and by maghemite nanoparticles deposition via evaporation process. Before the deposition process, the Constantan tapes are cleaned with diluted sulfuric acid 60% in distilled water and then are placed in an ultrasonic bath with acetone for 15min.

The deposition by plasma spraying method ("Sputtering") is a process which atoms are ejected from a solid material by bombardment with energetic particles (Behrisch, 1981). The Constantan tapes are positioned as substrate at the bottom of the support, becoming slightly anodized. The cathode, positioned at the upper part, consists of a molybdenum plate. All the procedures are made in the Federal University of Santa Catarina (LEPTEN/UFSC and LABMAT/UFSC).

The temperature, pressure, voltage and time (period of time that the sample is under the plasma influence) control during the process, allow the achievement of different sizes and distribution of nanoparticles. The parameters of control are presented in Table 1. The first samples, with a cycle of 30min. are called Mo_1 Nanostructure and the others prepared with a cycle of 1h are called Mo_2 Nanostructure.

Table 1. Parameters of control used in plasma process.

| | |
|-------------------------------|-----------------------------------|
| Voltage | 700V |
| Pressure | 3.67mbar |
| Threshold Temperature | 800°C |
| Flow | 180sccm* (90Ar/10H ₂) |
| Position – Floating Potential | Fluctuant Potential |

* sccm: standard cubic centimeters per minute.

The deposition of maghemite (γ - Fe₂O₃) on the heated surface was done by evaporation process with a nanoparticles suspension, consisting of water and maghemite nanoparticles. The process is accomplished by applying, with a syringe, a layer of this solution on the Constantan substrate. The tape is connected to a power source, which allows the surface heating and consequently, the evaporation of the liquid, leaving only the deposited nanoparticles.

The samples are prepared with two and four nanostructure maghemite layers, referred to Maghemite_1 Nanostructure and Maghemite_2 Nanostructure, respectively. It was performed a test with maghemite nanofluid on Constantan tape to compare with other experimental results and it was observed the deposition of maghemite on the substrate.

In order to determine the deposited layers on the surfaces, a method based on weight of samples with and without deposition was carried out. For the nanostructures case the true weight was considered as the difference between the weight of sample with deposition and the weight of the sample without deposition. With these values and the volume of the same, as well as the density (ρ) of each material supplied from the literature, it was possible to calculate the nominal thickness of the deposited layer, according to Eqs. (1) and (2).

$$\rho = \frac{m}{V} \quad (1)$$

$$V = A \cdot e \quad (2)$$

where A is the heated surface area (in contact with the working fluid) and e is the nominal of the deposited layer thickness.

2.3. Experimental Procedures

Before to fill the boiling chamber with the distilled water, used as working fluid, it was done the vacuum inside it. During the experiment, the temperature of the working fluid and the atmospheric pressure conditions were controlled by a forced flow of water in the space created between the glass tube of the boiling chamber and the plexy-glass wall of the external chamber.

Upon reaching the saturation temperature, each test started with heat flux imposed by controlling the electric current source, in order to increase it constantly until reaching the temperature stabilization. Therefore, when the heating surface temperature reached 100°C, the power source was turned on and adjusted initially to 3A. In the present work the heating mode was by increasing the heat flux until reaching the critical heat flux. When the critical heat flux is attained the surface temperature rises sharply leading to burnout. In this case the tape breaks up and this can hinder the current and the temperature decrease.

The data were monitored by LabView 6.1 software. The experiment was performed by heat flux imposed, through control of electrical current by the power source and the Constantan tape was heated directly by Joule effect. With the electrical resistance values and the area of the Constantan tape it was possible to calculate the heat flux corresponding to electrical current through the Power's Law, see Eq. (3). Thus, with the temperature values obtained by thermocouples in contact with the tape it was possible to calculate the heat transfer coefficient by Eq. (4).

$$q'' = \frac{Ri^2}{A} \quad (3)$$

$$h = \frac{q''}{(T_w - T_{sat})} \quad (4)$$

where R is the electrical resistance of the Constantan tape, i is the electrical current and A is the tape cross-sectional area. The temperatures data are selected in order to get an average of 100 points after of temperature stabilization for each electrical current imposed.

The visualization of the boiling process was done by a high speed camera, 1200hs PCO, capable of capturing 640 frames per second with the highest resolution (1024x1024). LEDs were used for providing good conditions of lighting.

2.4. Characterization of Samples

Before each test, the samples were characterized using the following different techniques:

i. Scanning electron microscopy (SEM) to obtain structural and chemical information. This procedure was performed using a scanning microscope Phillips XL30.

ii. Atomic force microscopy (AFM) in order to measure the roughness and to obtain the topographic images of the samples. The analyses were performed using the atomic force microscope Nanosurf EasyScan2 with Tapping operation mode. By this method it was possible to obtain the average roughness (R_a) for each surface.

iii. Samples with maghemite deposition could not be analyzed by AFM due to its high roughness, which could cause breakage of equipment. For this reason, the parameter R_a was determined using the SurfTest SS, 401model, with the same scanning area as the other samples.

iv. The wettability test by measuring the apparent static (θ_{pp}), advancing (θ_A) and receding (θ_r) contact angles. The device used was a goniometry OCA 20 from Dataphysics Company. It is used as fluid ultrapure water, deionized by a system DirectQ3 Millipore. The drops were analyzed by an algorithm ADSA (axysimmetric drop shape analysis).

The characterization measurements were done in the LABMAT/UFSC.

The surfaces tested by nanofluids maghemite boiling were also characterized after the tests, without cleaning to avoid the withdrawal of the maghemite layer deposited during the test.

Table 2 shows the different types of surfaces tested during the nucleate boiling of water.

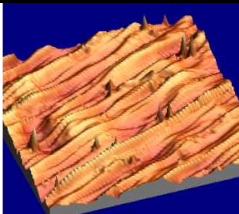
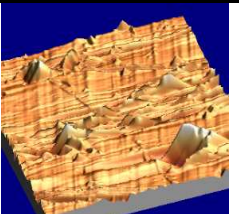
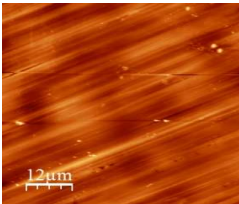
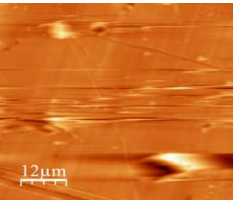
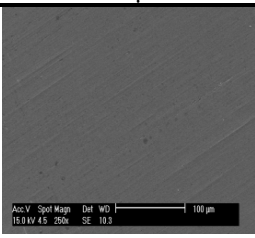
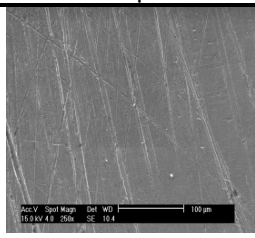
Table 2. Description of the tapes surfaces tested in this study.

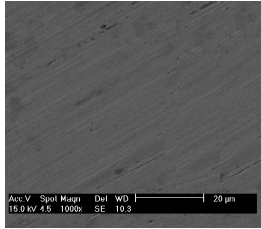
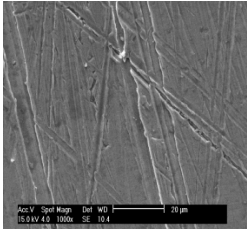
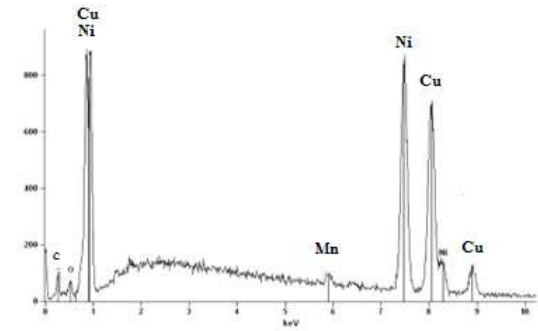
| | |
|---------------------------|--|
| Smooth Substrate | Constantan surface without deposition. Standard smooth surface. |
| Rough Substrate | Constantan surface without deposition. Higher roughness due to sanding process. |
| Mo_1 Nanostructure | Constantan surface with molybdenum deposition by Sputtering. Plasma exposure time = 30min. |
| Mo_2 Nanostructure | Constantan surface with molybdenum deposition by Sputtering. Plasma exposure time = 1h. |
| Maghemite_1 Nanostructure | Constantan surface with maghemite deposition by nanofluid evaporation process. With 2 deposited layers. |
| Maghemite_2 Nanostructure | Constantan surface with maghemite deposition by nanofluid evaporation process. With 4 deposited layers. |
| Maghemite Nanofluids | Constantan surface with maghemite deposition. |

2.4.1. Smooth and Rough Substrates

Table 3 shows the characterization of the Smooth and Rough Substrates. The substrate, a Constantan tape, is considered as smooth surface compared to the other samples. Their average roughness (R_a) was $0.02\mu\text{m}$ and the images obtained by AFM and SEM revealed a smooth surface with few topographic irregularities. The chemical analysis (EDX) showed the composition concerning the Constantan, composed of nickel and copper mostly and manganese and carbon, as residual material. The rough substrate surfaces showed roughness (R_a) of $0.17\mu\text{m}$ and it was found by AFM and SEM images an increase in the topographic irregularities.

Table 3. Results for the Smooth and Rough Substrate characterization.

| Characterization Techniques | Smooth Substrate | Rough Substrate |
|-----------------------------|---|---|
| AFM |  |  |
| |  |  |
| R_a | $0.02\mu\text{m}$ | $0.17\mu\text{m}$ |
| SEM |  |  |
| | 250x | 250x |

| | |
|---------------------------------|---|
| |   |
| | 1000x 1000x |
| EDX |  |
| Chemical Composition (% Weight) | Cu (48.53) Ni (45.01) Mn (1.21) C (4.76) |

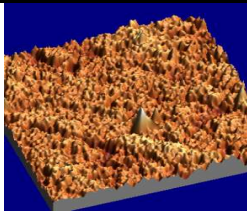
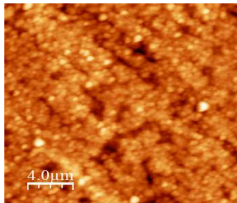
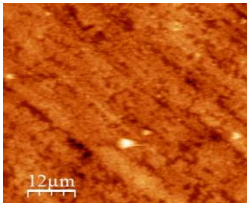
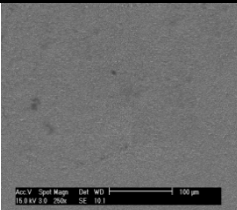
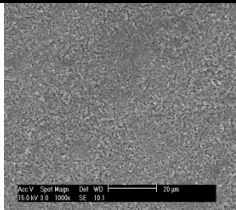
2.4.2. Molybdenum Nanostructure Surfaces

Tables 4 and 5 show the nanostructures of molybdenum characterization obtained by the Sputtering process. It was observed that the surfaces showed a deposition with fine-grained (average grain size lower than $0.5\mu\text{m}$) and homogeneous distribution. Through chemical analysis it was found the increase in the concentration of deposited particles, from 1.8% in Mo_1 Nanostructure to 9.83% in Mo_2 Nanostructure.

As a result of deposition, the roughness was also increased from $0.05\mu\text{m}$ for Mo_1 Nanostructure to $0.20\mu\text{m}$ for Mo_2 Nanostructure. The pictures obtained by AFM showed for the Mo_1 Nanostructure, a greater number of topographic irregularities compared to the smooth and rough substrate samples.

For the Mo_2 Nanostructure the images obtained by AFM showed a noise due to the high surface roughness of these samples, see Table 5. The test allowed calculating the R_a parameter, however, because the high roughness value it was not possible to record topographic pictures.

Table 4. Results for the Mo_1 Nanostructure characterization.

| Characterization Techniques | Mo_1 Nanostructure | |
|-----------------------------|---|---------------------------------|
| AFM |  | |
| |   | |
| R_a | 0.05 μm | |
| SEM |   | 250x 1000x |

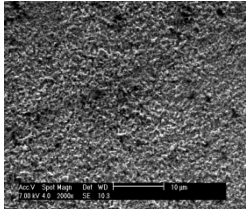
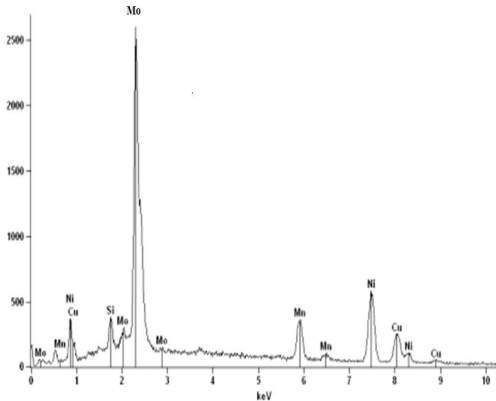
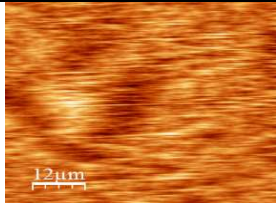
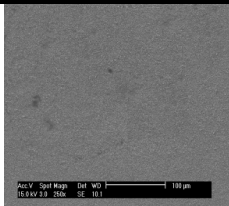
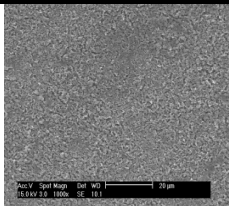
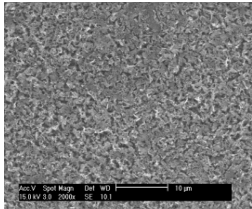
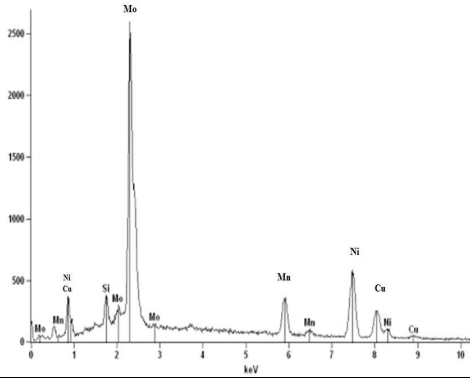
| | |
|---------------------------------|--|
| |  <p>2000x</p> |
| EDX |  |
| Chemical Composition (% Weight) | Cu (52.76) Ni (40.96) Mn (4.48) Mo (1.8) |
| Particle size deposited < 0.5μm | |

Table 5. Results for the Mo_2 Nanostructure characterization.

| Characterization Techniques | Mo_2 Nanostruture |
|---------------------------------|--|
| AFM |  |
| R_a | 0.20μm |
| SEM |  <p>250x</p>  <p>1000x</p>  <p>2000x</p> |
| EDX |  |
| Chemical Composition (% Weight) | Cu (49.26) Ni (40.51) Mn (0.41) Mo (9.83) |
| Particle size deposited < 0.5μm | |

2.4.3. Maghemite Nanostructure Surfaces

The results for Maghemite Nanostructures characterization by SEM, showed micro structural aspects with different grain sizes, porosity and heterogeneous distribution, see Table 6.

There was an increase in the Fe concentration, from 57.2% for Maghemite_1 Nanostructure to 97.5% for Maghemite_2 Nanostructure, see Table 7. Due to the high roughness, it was not possible to measure the R_a parameter by AFM method, therefore the roughness was obtained by rugosimeter and the values were 0.30 μ m and 0.35 μ m, respectively.

Table 6. Results for the Maghemite_1 Nanostructures characterization.

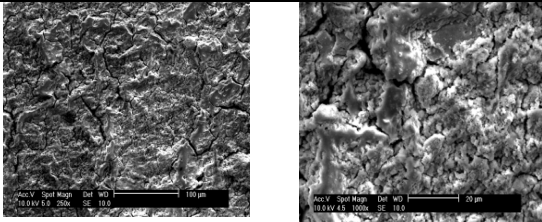
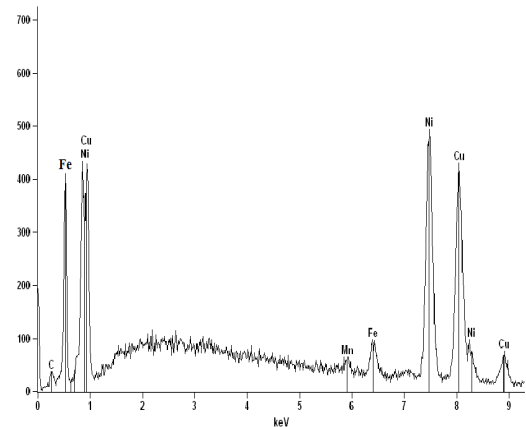
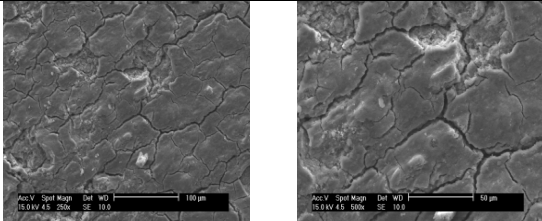
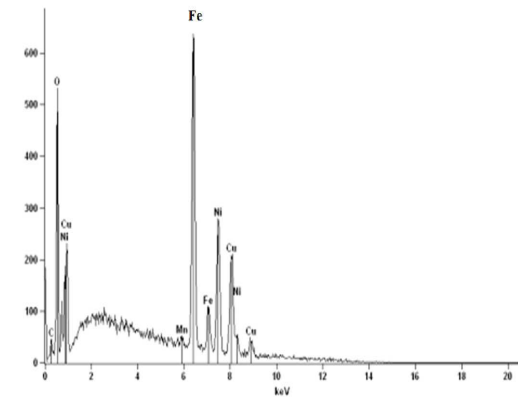
| Characterization Techniques | Maghemite_1 Nanostruture |
|---------------------------------|---|
| R_a | 0.30 μ m |
| SEM |  |
| EDX |  |
| Chemical Composition (% Weight) | Cu (29.54) Ni (13.31) Fe (57.15) |

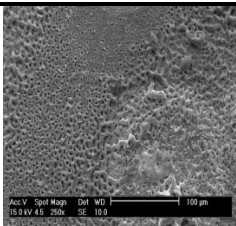
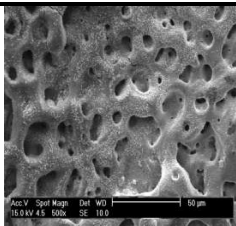
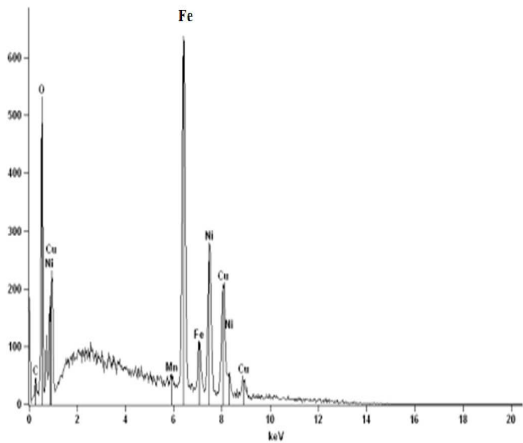
Table 7. Results for the Maghemite_2 Nanostructure characterization.

| Characterization Techniques | Maghemite_2 Nanostruture |
|---------------------------------|--|
| R_a | 0.35 μ m |
| SEM |  |
| EDX |  |
| Chemical Composition (% Weight) | Cu (1.21) Ni (1.29) Fe (97.5) |

2.4.4. Maghemite Nanofluids

Table 8 shows the deposition from the test with maghemite nanofluid showed a surface with higher porosity and higher Fe concentration (99.1%) compared to the nanostructure surfaces. The R_a parameter was $0.38\mu\text{m}$.

Table 8. Results for the Maghemite Nanofluids characterization.

| Characterization Techniques | Maghemite Nanofluid | |
|---------------------------------|---|---|
| R_a | $0.38\mu\text{m}$ | |
| SEM |  |  |
| | 250x | 1000x |
| EDX |  | |
| Chemical Composition (% Weight) | Cu (0.94) Ni (0.99) Fe (99.09) | |

2.4.5. Contact Angle

The surface characteristics of the samples were analyzed by wettability test, which provides the static (θ), receding (θ_r) and advancing (θ_a) contact angles.

Table 9 shows the results for smooth and rough substrates. It was observed that the Constantan, which was the material used as substrate, presented partial wettability characterizing a hydrophilic behavior. The contact angle hysteresis is observed as a result of the surface heterogeneity. However, the rough substrate samples showed a hydrophobic behavior, i.e., with static contact angle higher than 90° .

Table 9. Wettability test results for the smooth and rough substrate.


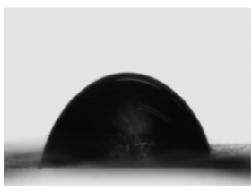




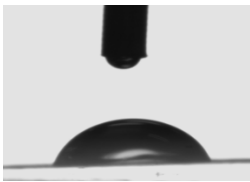
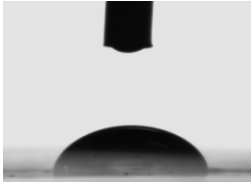


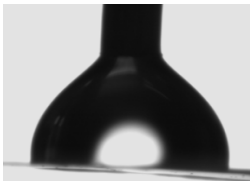

| Contact Angles | Smooth Substrate | Rough Substrate |
|----------------|--|---|
| Static |  75° |  96° |
| Receding |  49° |  75° |
| Advancing |  68° |  93° |

Table 10 shows the contact angles for Mo_1 Nanostructure and for Mo_2 Nanostructure, where it was observed a hydrophilic behavior.

With the nanoparticles deposition was observed a reduction in the static and receding contact angle. It was also observed that the contact angle hysteresis increased for the nanostructures. This is due to the higher irregularity and heterogeneity of these surfaces.

Table 10. Wettability test results for Mo_1 Nanostructure and Mo_2 Nanostructure.

| Contact Angles | Mo_1 Nanostructure | Mo_2 Nanostructure |
|----------------|--|---|
| Static |  64° |  62° |
| Receding |  49° |  41° |
| Advancing |  68° |  82° |

Surfaces with maghemite deposition showed an increase in the wettability, with hydrophilic behavior for all tests, especially for Maghemite_2 Nanostructure and Maghemite Nanofluids which static contact angles were close to zero. For these samples, it was no possible to observe the advancing and receding angles due to the low values, see Tables 11 and 12.

Table 11. Wettability test results for Maghemite_1 Nanostructure and Maghemite_2 Nanostructure.





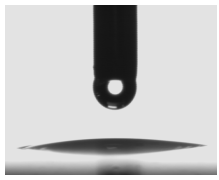
| Contact Angles | Maghemite_1 Nanostructure | Maghemite_2 Nanostructure |
|----------------|--|--|
| Static |  43° |  0° |
| Receding |  38° | <10° Completely Wetting |
| Advancing |  80° | <10° Completely Wetting |

Table 12. Wettability test results for Maghemite Nanofluids.

| Static Contact Angle | Receding Contact Angle | Advancing Contact Angle |
|----------------------|------------------------|-------------------------|
|----------------------|------------------------|-------------------------|

| | | |
|---|-----------------------------------|-----------------------------------|
|  | $<10^\circ$ Completely Wetting | $<10^\circ$ Completely Wetting |
|---|-----------------------------------|-----------------------------------|

3. BOILING CURVES

Figures 3 to 7 show the experimental points for the nucleate boiling regime with saturated water. For all cases, the points of maximum heat flux represent the heat flux which occurs the fusion of the material tape, i.e., the critical heat flux (CHF).

Figure 3 shows the experimental points for the smooth and rough substrate. It was observed an increase in the CHF for rough surface, of 19%, and the heat transfer coefficient increased significantly, about 10% for 753kW/m^2 .

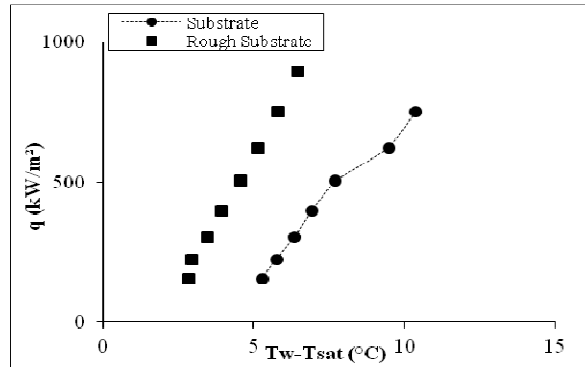


Figure 3. Boiling curves for smooth and rough substrate.

Figure 4 shows the results for molybdenum nanostructure and for smooth substrate. The critical heat flux increased about 19% over the smooth substrate, similar increase was observed for the roughness substrate compared to smooth substrate. The heat transfer coefficient showed different behaviors for low and high heat fluxes: for low heat flux the heat transfer coefficient decreased and for high heat flux the h increased.

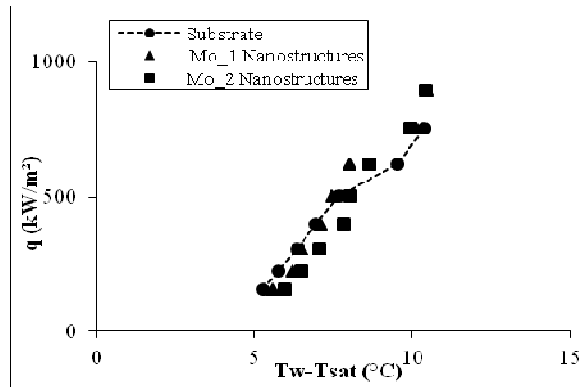


Figure 4. Boiling curves for smooth substrate and for molybdenum nanostructure.

Figure 5 presents the results for maghemite nanostructure surfaces and for smooth substrate. There was a significant increase in the CHF, about 139% for Maghemite_1 Nanostructure and 198% for Maghemite_2 Nanostructure, compared to the smooth substrate. The experimental points for Maghemite_1 Nanostructure and for Maghemite_2 Nanostructure were shifted to the left indicating a better heat transfer coefficient. For heat fluxes higher than 753kW/m^2 , it was observed the enhancement of the boiling for Maghemite_1 Nanostructure.

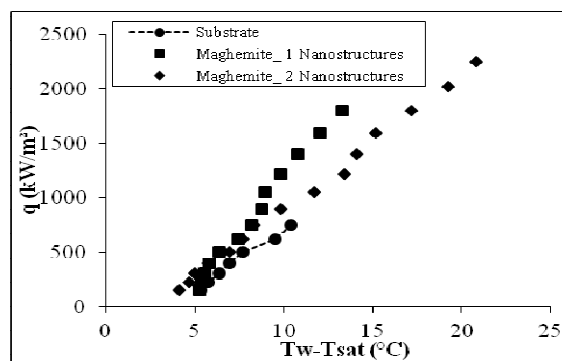


Figure 5. Boiling curves for smooth substrate and maghemite nanostructures.

Figure 6 shows the results for Maghemite_1 Nanostructure, for Maghemite_2 Nanostructure and for maghemite deposited during the boiling of the maghemite nanofluid. It was observed that there were no differences between the results for the maghemite nanofluid and those obtained for Maghemite_2 Nanostructure, which has four maghemite layers. For the nanostructure surface with two maghemite layers, called Maghemite_1 Nanostructure, there was a significant enhancement of the heat transfer coefficient for heat fluxes higher than 896 kW/m^2 .

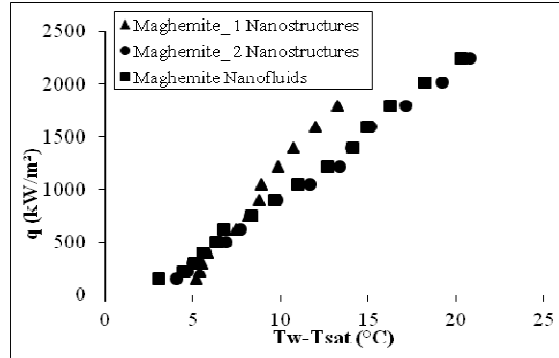


Figure 6. Boiling curves for maghemite nanostructure and maghemite nanofluid.

Figure 7 shows the results for the nucleate boiling on the smooth substrate and three surfaces having the same type of roughness substrate: the first one without deposition and the two others with deposition of molybdenum layer and maghemite layer, respectively. The nanoparticles deposition compared to roughness substrate without deposition, causes a decrease in the heat transfer coefficient. However, the experimental points for the surface with maghemite deposition are shifted to the left, indicating a better heat transfer coefficient. The deposition of molybdenum and maghemite were provided by using the same preparation procedure (Sputtering and evaporation techniques, respectively).

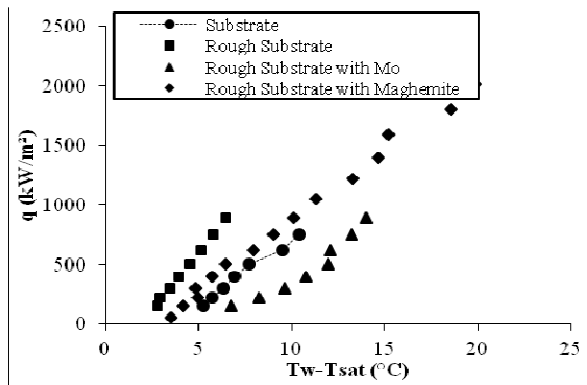


Figure 7. Boiling curves for smooth and rough substrate and rough substrate with nanoparticles deposition.

A summary of the results is presented in Table A.1 of Appendix A, including the values of the nominal deposited nanoparticles thickness, average roughness, contact angle, CHF and qualitative information about the coefficient of heat transfer.

Figure A.1 of Appendix A shows pictures obtained for the smooth substrate, Mo_1 Nanostructure and Maghemite_1 Nanostructure. It was observed an increase in the size of the vapor bubbles and a decrease in the bubbles release, for the nanostructures case and for the same heat fluxes. As a result, the necessary conditions for the CHF are delayed and the values are significantly high for the nanostructure surface compared to the smooth substrate.

4. DISCUSSION

4.1. Effect of nanostructures on heat transfer in nucleate boiling

Studies about the heat transfer in the boiling process indicate that the trapping of gases and vapor in the cavities of the heated surface promotes the onset of the nucleate boiling with less superheating, and surfaces that are not completely wetted will contain greatest amount of trapped gas, facilitating the heat transfer. Carey (1992) explained that for a superheating, a cavity will be activated if its radius of curvature (r_{\min}) is higher than a critical value (r^*), calculated by Eq. 5.

$$r^* = \frac{2\sigma T_{\text{sat}} v_{lv}}{h_{lv}(T_w - T_{\text{sat}})} \quad (5)$$

where σ , T_{sat} , v_{lv} , h_{lv} and T_w represent the surface tension (N/m), the saturation temperature of the fluid, the difference of the specific volume of the vapor and liquid phases, the latent heat of vaporization and the absolute temperature of the surface, respectively.

According to Carey (1992) each cavity has a specific r_{\min} , which is a function of its geometry and contact angle.

Nanostructured surfaces are characterized by the deposition of small nucleated particles and grown via the gas phase on a substrate. The presence of these nanoparticles (or nanoparticles clusters) on the substrate surface introduces a substantial change in the roughness. In the material are created, a lot of valleys between the deposited particles.

The effect of particles deposition on the substrate surface is to change the roughness and this interferes in the capacity of trapping vapor bubbles between particles (or nanoparticles) adjacent, i.e., in the "valley" left between two adjacent particles. The particles deposition leads to change of the surface tension as a function of the radius of curvature on the surface created by these particles. The smaller the particles the smaller radius of curvature, reaching nanoscale dimensions. Thus, although the nanoparticles deposited can create potential nucleation sites for the heat transfer, they can have a small radius of curvature, smaller than the critical radius required to activate the cavities.

The surface tension of a solid is the result of bond strength (or binding energy) between atoms which is a function of interatomic distance (r), so as the smaller the interatomic distance the highest the surface energy.

As already mentioned, the results obtained with the nanostructures showed an increase in heat transfer coefficient only for high heat fluxes and more remarkable in the maghemite case. Through the SEM images, it was possible to observe that in the molybdenum deposition was created a refined microstructure with particle sizes smaller than the maghemite nanostructures, as shown in Figure 8.

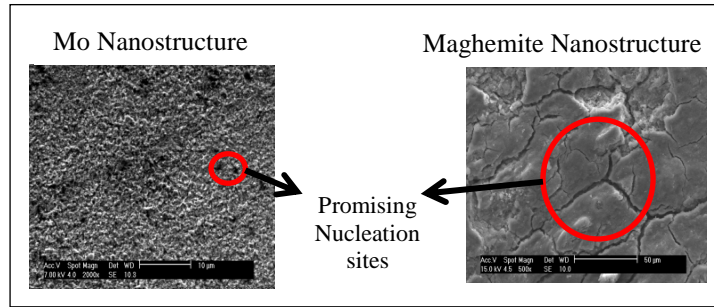


Figure 8. SEM images comparison for the molybdenum and maghemite nanostructures.

This configuration may therefore hinder the trapping of gases and reduce the heat transfer. However, according to Carey (1992), although the smaller cavities require a high superheating to start the nucleation, when it starts the superheating required to keep the vapor bubbles is smaller. This could explain the increase in the heat transfer coefficient for high heat fluxes obtained by nanostructures.

Figure 9 shows the comparison between the smooth substrate, rough substrate and nanostructures surfaces.

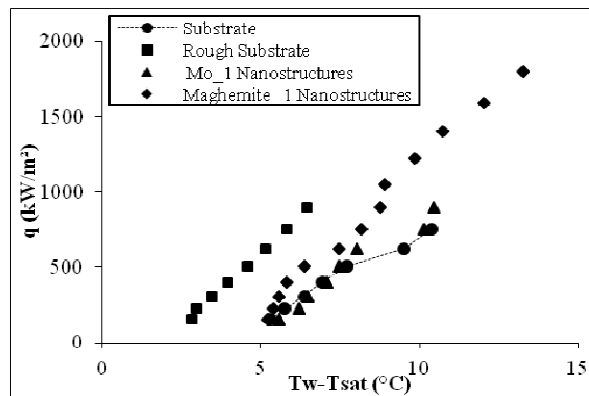


Figure 9. Comparison of boiling curves for the smooth and rough substrate and nanostructure surfaces.

It was observed that the rough surface showed an increase in the heat transfer coefficient. As this surface has no nanoparticles deposition, the cavities and surface defects are promising nucleation sites. However this surface showed a hydrophobic behavior, while the other analyzed surfaces showed a hydrophilic behavior. This can be explained by the fact that the rough surface has a lower amount of valleys and a lower surface tension, consequently, the less wettability. As a result, the promising nucleation cavities are not flooded with the liquid, allowing the trapping of gases which contributes to the nucleation sites activation and consequently, to heat transfer increasing.

In summary, it is suggested that the microstructural nanostructures surfaces influence the heat transfer process, so that its surface defects can be treated as nucleation sites and factors such as size and quantity of these are important. Moreover, surfaces with hydrophobic behavior have a highest heat transfer coefficient and the surface wettability also results from the surface defects configuration.

4.2. Effect of nanostructures on the critical heat flux

Nanostructures analyzed showed a reduction in the static and receding contact angle and an increase in the critical heat flux. The maghemite nanostructure showed a completely wetting surface and a high CHF compared to other analyzed surfaces.

The wettability increasing of nanostructures can also be explained by the increase of the number of surface defects, which increase the adhesion tension and consequently the increase of their interaction with the fluid. It is believed that hydrophilic surfaces allow the contact of the liquid on the heating surface for longer time, hindering the dryout and delaying the necessary conditions for the onset of critical heat flux phenomenon and burnout.

It was observed that in the nanostructure surfaces there is a smaller number of bubbles at the beginning of nucleate boiling, but with larger diameter. For heat fluxes close to CHF it was observed that the vapor bubbles for the nanostructures case were significantly higher than for the smooth substrate case.

Figure 10 shows vapor bubbles with larger diameter for high heat flux values, before the occurrence of the CHF. This picture suggests that these larger bubbles can be supplied by small steam columns as postulated by Haramura and Katto (1983) in the macrolayer model for the CHF.



Figure 10. Pictures obtained by high-speed camera.

In this analysis, although it was showed important changes in the contact angle as a function of surface defects imposed by nanostructures, there was another factor that could be contributing to the wettability increasing. Considering only this effect, would be expect a higher wettability for the molybdenum deposition case compared to the maghemite case. An important difference between these two nanostructures was the deposition layer resulting from their manufacturing processes used, which can lead to an increase in the surface roughness for the surfaces with higher deposition.

It is known that the surface roughness influences the boiling process, as postulated by Mikic and Rohsenow (1969) in studies on the nucleate boiling considering the heating surface effects.

It is suggested that there are contributions from two effects, the increase in the wettability as a result of the defects imposed by nanostructures and also the roughness imposed by nanoparticles deposition.

5. CONCLUSIONS

This study presents experimental results for nucleate boiling on Constantan nanostructure surfaces of molybdenum, by Sputtering process, and maghemite, by nanofluid evaporation technique. The experiment was performed at saturation temperature of water (100°C), used as working fluid, and at atmospheric pressure.

The main conclusions are:

- i. Nanostructures surfaces showed higher wettability, as a consequence of the greater number of surface defects imposed by nanoparticles;
- ii. The maghemite nanostructure surfaces showed more porosity and roughness. These samples have a nanoparticles layer thickness higher and, consequently, a higher wettability compared to molybdenum samples, suggesting that the roughness and thickness of the deposited layer also contributes to increasing the surface tension;
- iii. The molybdenum deposition samples, obtained by Sputtering process, showed a homogeneous distribution with nanoparticles size smaller than 5 μ m and hydrophilic characteristics;
- iv. The rough substrate showed a hydrophobic behavior, while the other samples with nanoparticles deposition showed a hydrophilic behavior;
- v. The nanostructures showed an increase in the CHF, especially for the case with maghemite deposition;
- vi. The critical heat flux increased as wettability increasing. It was observed an increase in the CHF as the static and receding contact angle decreasing;
- vii. The rough substrate samples showed an enhancement in the heat transfer coefficient, while others samples showed an increase in the h for high heat fluxes;
- viii. The surfaces with hydrophobic behavior influence the heat transfer coefficient positively. The promising nucleation cavities are not flooded with the liquid, allowing the trapping of gases which contributes to the nucleation sites activation and consequently, to heat transfer increasing;
- ix. Surface defects in the material affect the surface tension and therefore may influence the heat transfer mechanisms and the critical heat flux. The nanostructures have greater number of these defects imposed by the small nanoparticles size.

It is possible to conclude that the nanostructures have a great influence on the nucleate boiling process. Therefore, the small particles sizes in the nanostructures promote remarkable changes in the wettability which is function of the topography of substrate and the deposition.

6. ACKNOWLEDGMENTS

The authors gratefully acknowledge the support by CAPES (PROENG and NANOBIOTEC Projects) and CNPq. The authors also extend their gratitude to Mr. A. J. C. PACHECO, Mr. A. Oliveira and Mrs. B. C. P. MORASTONI for their important contribution to the laboratory work.

7. NOMENCLATURE

Alphabetic

| | | |
|-----------------|--------------------------------------|-----------------------|
| SEM | Scanning electron microscopy | |
| DRX | Energy-dispersive X-ray spectroscopy | |
| AFM | Atomic force microscopy | |
| sccm | Cubic centimeter per minute | |
| h | Heat transfer coefficient | [kW/m ² K] |
| h _{lv} | Latent heat of vaporization | [kJ/kg] |
| v | Velocity | [m/s] |
| k | Thermal Conductivity | [W/mK] |
| L | Characteristic length | [m] |
| Na | Active nucleation sites density | [m ²] |
| Q | Heat rate | [W] |
| q | Heat flux | [kW/m ²] |
| r | Characteristic radius of the cavity | [m] |
| R | Electrical resistance | [Ω] |
| Ra | Average roughness | [μm] |
| Tsat | Saturation temperature of the fluid | [°C] |
| Tw | Surface temperature | [°C] |
| V | Electrical voltage | [V] |
| i | Electrical current | [A] |
| f | Frequency | [Hz] |

Greek Letters

| | | |
|---|--------------------|----------------------|
| θ | Contact angle | [°] |
| ρ | Density | [kg/m ³] |
| μ | Absolute viscosity | [kg/ms] |
| σ | Surface tension | [J/m ²] |
| υ | Specific volume | [m ³ /kg] |

Subscripts

| | |
|-----|----------|
| b | Bubble |
| l | Liquid |
| v | Vapor |
| s | Solid |
| c | Critical |
| max | Maximum |

8. REFERENCES

- AHN, H.S., LEE, C., KIMB, H., JO, H., KIMB, H., JO, H., KANG, S., KIMA, J., SHIN, J., KIMA, M.K., *Pool boiling CHF enhancement by micro/nanoscale modification of zircaloy-4 surface*, Nuclear Engineering and Design 240, 350–3360, 2010.
- BANG, I.C., CHANG, S.H., *Boiling heat transfer performance and phenomena of Al₂O₃ – water nano-fluids from a plain surface in a pool*, Int. J. Heat and Mass Transfer, 48, 2407 – 2419, 2005.
- BEHRISCH, R., *Sputtering by Particle bombardment*, Springer, Berlin, 1981.
- CAREY, V.P., *Liquid-vapor phase-change phenomena*, Taylor & Francis, USA, 1992.
- CHOI, U.S., *Developments and Applications of Non-Newtonian Flows*, ASME FED-Vol. 231/MD, vol. 66, pp. 99–105, 1995.
- FORREST, E., WILLIAMSON, E., BUONGIORNO, J., HU L.W., RUBNER, M., COHEN, R., *Augmentation of nucleate boiling heat transfer and critical heat flux using nanoparticle thin-film coatings*, Int. J. Heat and Mass Transfer, 53, 58–67, 2010.
- GOLUBOVIC, M.N., HETTIARACHCHI, H.D.M., WOREK, W.M., MINKOWYCZ, W.J., *Nanofluids and critical heat flux, experimental and analytical study*, Applied Thermal Engineering 29, 1281–1288, 2009.
- HARAMURA, Y., KATTO Y., *A new hydrodynamic model of CHF applicable widely to both pool and forced convection boiling on submerged bodies in saturated liquids*, International Journal of Heat Mass Transfer, vol. 26, pp. 389–399, 1983.
- HENDRICKS, T.J., KRISHNAN, S., CHOI, C., CHANG, C., PAUL, B., *Enhancement of pool-boiling heat transfer using nanostructured surfaces on aluminum and copper*, International Journal of Heat and Mass Transfer, vol 53, pp. 3357–3365, 2010.
- KIM, H.D., KIM, J.B., KIM, M.H., *Experimental studies on CHF characteristics of nano-fluids at pool boiling*, Int. J. Multiphase Flow, 33, 691 – 706, 2007.
- KIM, J., *Review of nucleate pool boiling bubble heat transfer mechanisms*, International Journal of Multiphase Flow, vol. 35, pp. 1067–1076, 2009.
- MIKIC, B. B. ROHSENOW, W. M., *A new correlation of pool boiling data including the effect of heating surfaces characteristics*, ASME Journal of Heat Transfer, vol. 9, pp 245–250, 1969.
- STUTZ, B., SILVEIRA, C.H., MORCELI, Da Silva, M.M.F., Cioulachtjian, S., Bonjour, J., *Influence of Nanoparticle Surface Coating on Pool Boiling*, Experimental Thermal and Fluid Science, 2011.
- WEN, D., DING, Y., *Experimental investigation into the pool boiling heat transfer of aqueous based γ-alumina nanofluids*, Journal of Nanoparticle Research 7: 265–274. 2005.

APPENDIX A

Table A.1. A summary of the experimental results.

| Surfaces | Nominal thickness (μm) | R_a (μm) | θ ($^\circ$) | θ ($^\circ$) | θ ($^\circ$) | CHF (kW/m^2) | h behavior |
|--------------------------------|-------------------------------------|-------------------------|-----------------------|-----------------------|-----------------------|-------------------------|--|
| Smooth Substrate | --- | 0.02 | 75 | 49 | 68 | 753 | Reference |
| Rough Substrate | --- | 0.17 | 96 | 75 | 93 | 896 | Enhancement |
| Nanostructure Mo_1 | 5 | 0.05 | 64 | 44 | 90 | 896 | Degradation for low heat flux value and enhancement for high heat flux value |
| Nanostructure Mo_2 | 7 | 0.20 | 62 | 41 | 81 | 896 | Degradation for low heat flux value and enhancement for high heat flux value |
| Nanostructure Maghemite_1 | 3 | 0.30 | 43 | 38 | 80 | 1798 | Enhancement for high heat flux value |
| Nanostructure Maghemite_2 | 13 | 0.35 | 0 | < 10 | < 10 | 2246 | Enhancement for high heat flux value |
| Maghemite Nanofluid | 14 | 0.39 | 0 | < 10 | < 10 | 2246 | Enhancement for high heat flux value |
| Rough Substrate with maghemite | 13 | 0.23 | 40 | < 10 | < 10 | 2246 | Degradation |
| Rough Substrate with Mo | 6 | 0.41 | 51 | 37 | 85 | 896 | Degradation |

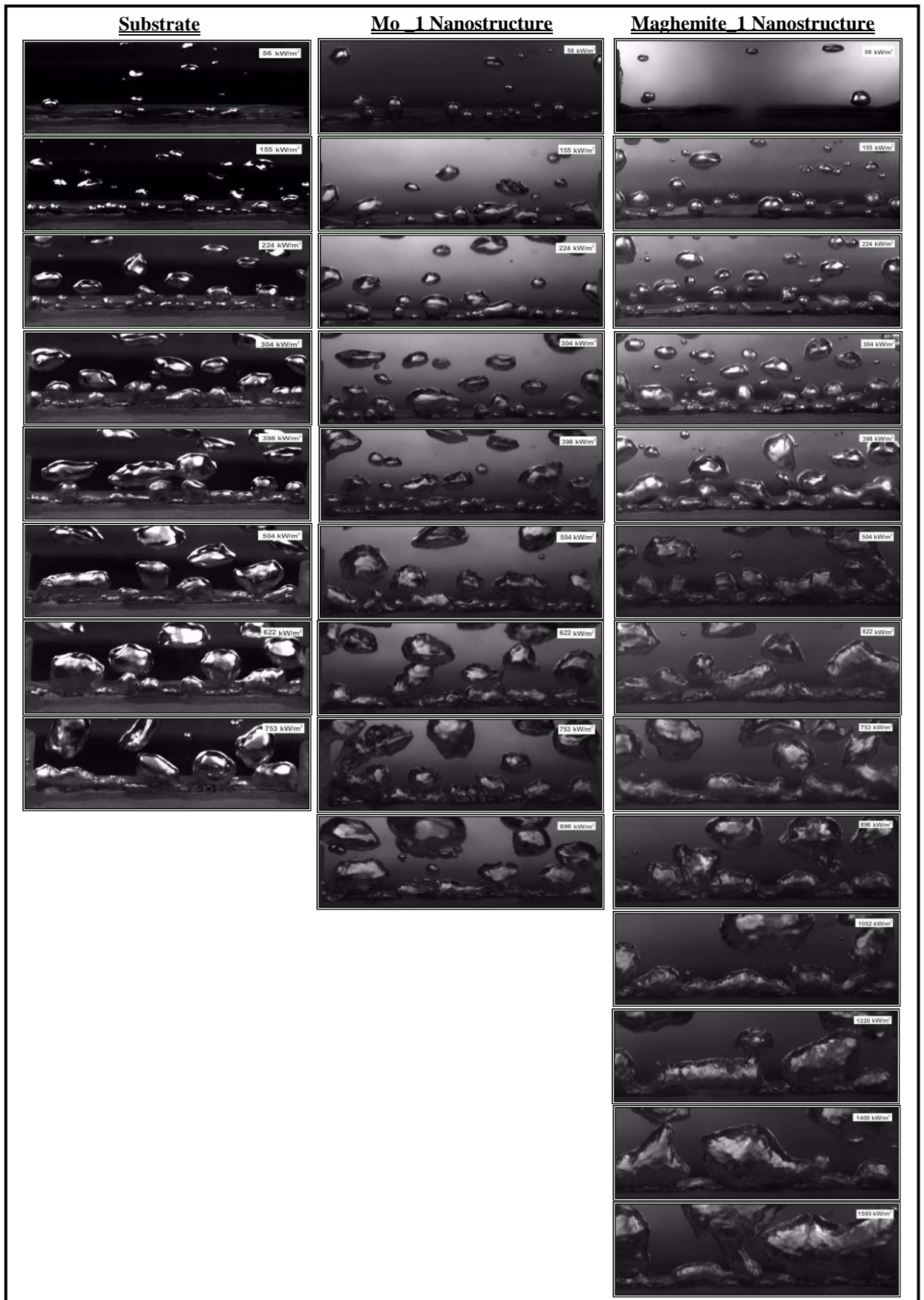


Figure A.1. Pool boiling visualization for Smooth Substrate, Mo_1 Nanostructure e Maghemite_1 Nanostructure.